International Journal of Materials Science and Applications
2022; 11(2): 55-61
http://www.sciencepublishinggroup.com/j/ijmsa
doi: 10.11648/j.ijmsa.20221102.13
ISSN: 2327-2635 (Print); ISSN: 2327-2643 (Online)

Failure Analysis Report on Fractured Torsion Bar in Suspension of a Vehicle

Nan Nan[1, *], Jijun Feng[2]

[1]School of Science, Hubei University of Automotive Technology, Shiyan, China

[2]Technical Center of Dongfeng Commercial Vehicle, Dongfeng Motor Corporation, Wuhan, China

Email address:

nann_lxy@huat.edu.cn (Nan Nan), fengjijun@dfcv.com.cn (Jijun Feng)

[*]Corresponding author

To cite this article:

Nan Nan, Jijun Feng. Failure Analysis Report on Fractured Torsion Bar in Suspension of a Vehicle. *International Journal of Materials Science and Applications.* Vol. 11, No. 2, 2022, pp. 55-61. doi: 10.11648/j.ijmsa.20221102.13

Received: March 29, 2022; **Accepted**: April 20, 2022; **Published**: April 28, 2022

Abstract: Accidents caused by fractured torsion bars in off-road vehicles (ORVs) have occurred during road tests. Through visual inspection of the fracture in the failed samples, the preliminary conclusion is that the typical torsional fracture occurs according to its ratchet shape and 45-degree cracking direction to the bar axis. The crack initiated at the side surface of the fillet on the spline end. All failed parts during road tests have identical fracture modes and crack initiation sites, which implies that they have identical failure reasons. Techniques such as scanning electron microscopy (SEM), metallographic observation, hardness test and spectral component analysis have been performed to obtain detailed information to diagnose the cause of failure. The result reveals that the fracture was caused by fatigue cracking initiated from the spline fillet. In addition, SEM images of the intergranular feature of the fracture initiation zone demonstrate that the untimely formation of a fatigue core and very quick expansion of the crack directly result from over-brittleness. This behavior can be ascribed to insufficient tempering after the quenching process, which was confirmed by a tempering simulation experiment: after the tempering experiment, the artificial struck fracture of the sample became a 100% dimple fracture, and the hardness distribution became more uniform and reasonable. Thus, the brittleness was eliminated, and the strength was ensured after an expanding tempering time. This investigation can provide reference value for solving and preventing such types of failures.

Keywords: Torsion Bar, Spline, Fatigue, Over-brittleness, Tempering

1. Introduction

The torsion bar spring is the key component in vehicle suspension that provides ride comfort through elastically connecting the wheels and vehicle frame [1-3]. To ensure strength and toughness, super-high-strength steel 45CrNiMoVA is generally accepted as the suitable material to manufacture vehicle torsion bars. Torsion bars usually require heating treatments, such as quenching and subsequent tempering, to obtain the required microstructures and further reinforcement treatments, such as pre-twist and surface rolling [4]. In addition, a phosphating process is required to enhance the wear resistance [5]. The related process is shown in Figure 1.

Failure occurred when the road test mileage reached 1661~2500 km, which corresponds to approximately 10^4 ~10^5 cycles of cyclic torsion, and cracking of the torsion bar was diagnosed as the main cause after a dissembling inspection. The crack origin is located at the spline on the small end of the torsion bar, as illustrated in Figure 2 (indicated by a red arrow), and all cases have identical fracture modes, which implies that there must be an inherent commonality. This paper presents the techniques and procedures that were used to diagnose the cause of failure.

Figure 1. *Heating treatments and reinforcement treatments for torsion bar.*

Figure 2. *Crack position on torsion bar spline.*

2. Experimental Methods

2.1. Layout for Failure Analysis

To facilitate the systematical failure analysis, one fractured torsion bar in a left axle during the road test (S1) was selected as the main analysis object, and another fractured bar in the same batch during the fatigue test, which has similar cycles of fatigue life to the failure mileage of S1, was selected as the reference (S2, life time: 7×10^4). The sample numbering information is shown in Table 1.

Table 1. *Sample details of different number.*

Sample number	Description
S1	Target sample for failure analysis after road test
S2	Referencing control sample failed during fatigue test

2.2. Instrumental Techniques

General information on crack propagation can be obtained from macroscopic observations of the fracture surface, including the crack source, propagation direction and simple stress conditions. The microstructure of concerned regions on the failed surface was observed by scanning electron microscopy (SEM, Hitachi SU-70); the metallographic structure was observed by optical microscopic examination. The microhardness measurement of the cross section was performed by a Vickers system with a load of 1000 g. The chemical composition of the shaft part was analyzed by an Optical Emission Spectrometer (OES), and the tempering property of the product was examined by the tempering simulation experiment based on the producer's requirement, where a muffle furnace was used for the heat treatment.

3. Results of Investigations

3.1. Visual Inspection on the Fracture Surface

There are secondary cracks near the main crack initiation excluding the part that has already cracked, and these cracks have an irregular pattern. The main crack is disassembled for further information on the failed surface. The fracture morphologies of S1 and S2 are shown in Figure 3. The main fractures of S1 and S2 initiated from the place marked by the red arrow in Figures 3a and 3b. The fracture sources and adjacent areas appear to be quite brittle. The fracture initiation site is on the spline part, which is approximately 10 mm from the joint place between spline tail and shaft, as observed from the side view.

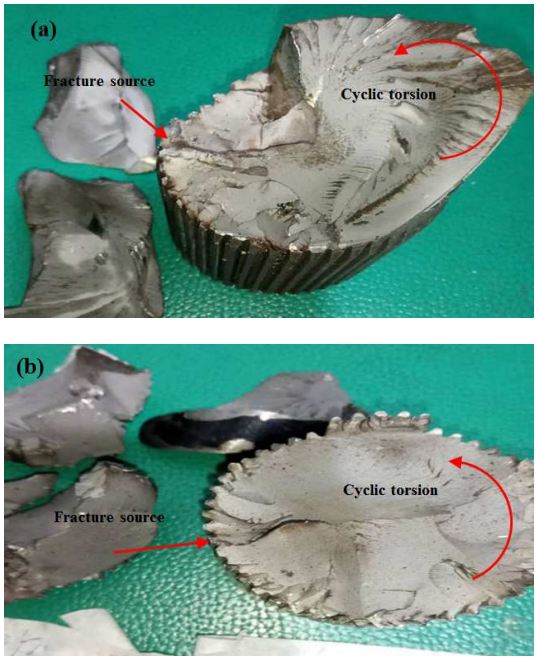

Figure 3. *Morphology of main fractures of samples, (a) S1, (b) S2.*

The fracture of S1 appears to be very informative, as shown in Figure 3a. The fracture of S1 exhibits a ratchet pattern and a 45° inclination, which is easily identified as a torsional fatigue fracture that failed under alternating torsional stress, since a ratchet pattern is a typical feature of torsional fatigue fracture [6, 7]. This is a mixed fracture, and the stair-step phenomenon is generally explained by the combined effect of maximum direct stress and shear stress. Some distributed secondary cracks are also found, which extended into the internal part of the fracture of S1. S2 has a similar fracture morphology to S1: S2 exhibits the ratchet feature, but it has a less obvious 45° inclination, as shown in Figure 3b, which is still proven to be torsional fatigue fracture.

Additionally, the part fracture can be perfectly matched with its counterpart, which indicates that they are macroscopic brittle, although it might reveal a deep result on the microscopic scale.

In summary, all fractures initiated from the same place at the fillet part of the spline and ultimately failed under alternating torsion. Furthermore, torsional fatigue features were discovered on the fracture of S1 and S2. From this viewpoint, the fatigue source is usually sensitive to the stress concentration, which easily occurs at the spline root and sometimes a notch, manufacturing defect or improper structure design [8-11].

3.2. SEM Inspection on Fracture Surface

The crack source area of the samples was cut into proper size using wire-electrode cutting for SEM inspection.

3.2.1. SEM Analysis of S1

The SEM image of the fracture source region of S1 is shown in Figure 4. Characteristics of grinding and rough marks are shown in Figure 4a. A large proportion of intergranular areas was also noticed in this region which indicates that this area is very brittle. However, such brittleness is usually considered a deficiency for torsion bars, which implies mechanical degradation. Instead, a dimple feature of the area is desirable. As shown in Figure 4b, the grain boundary surfaces are clear and clean and no microscopic features, such as cross feet or obviously distributed micro holes, were found on these surfaces; thus, the possibility of hydrogen embrittlement and harmful precipitates at the grain boundary (temper brittleness) should be excluded. Fatigue fracture usually exhibits transgranular features, and fatigue striations can be found in many cases. However, intergranular fracture can form on fatigue fractures as if it is a complete static–load fracture for high-strength steels if the tensile stress is very high or the material is brittle [12, 13]. In other words, S1 is only a particular case, since its macroscopic fracture exhibits the fatigue feature as mentioned in the macroscopic observation part, and the failure life of S1 is close to that of S2 after mileage conversion. The area of the fatigue expansion zone is quite small that it only covers a distance of approximately 10 mm to the surface, which indicates a high stress condition.

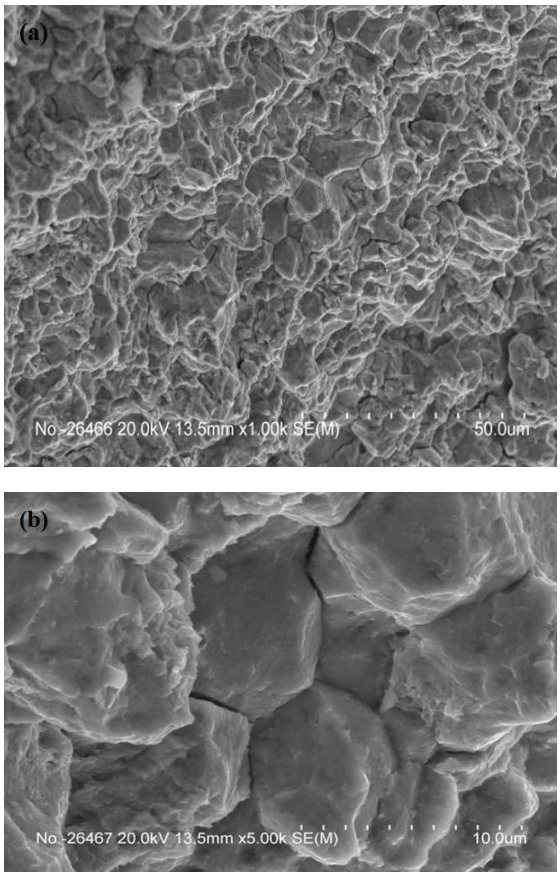

Figure 4. *SEM images of fracture source region of S1: (a) Low magnification (b) High magnification of intergranular area.*

In regions relatively far away from the fatigue expansion zone (approximately 20 mm to the crack initiation point), the fracture begins to exhibit mixed features of the intergranular section and very small areas of dimples (Figure 5). Despite the ductile property of dimples, the brittle fracture still dominates, which strongly proves the inhomogeneity of the microstructure caused by inadequate tempering, since the torsion bar experiences an integral heat treatment.

The crack initiation area (spline root near the main fracture) was also inspected to check whether there were manufacturing defects, but it was smooth, no such defects were detected, and the transition of the fillet position was geometrically normal.

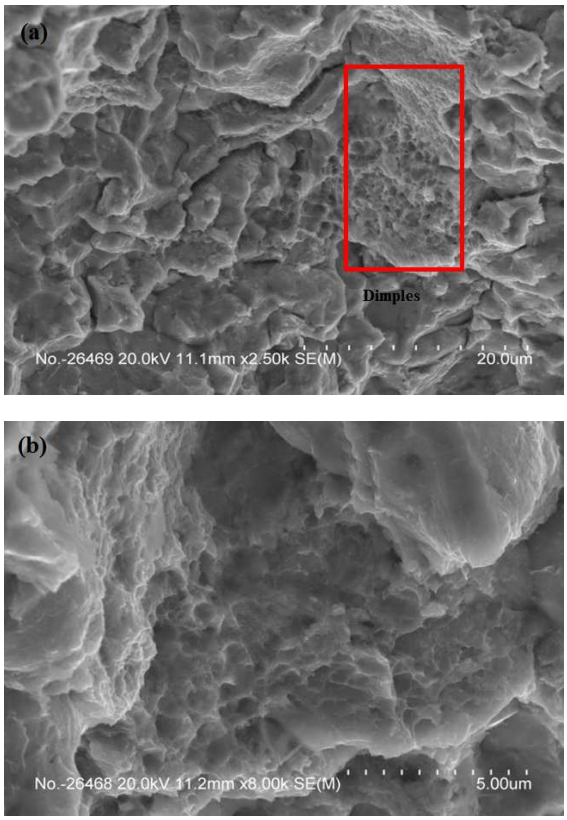

Figure 5. *Mixed fracture of intergranular section and dimples away from fatigue propagation area on S1: (a) Low magnification (b) High magnification of dimples.*

3.2.2. SEM Analysis of S2

S2 is our referencing control sample from the fatigue test, the fracture source of S2 is shown in Figure 6a. The crack of S2 initiated from the same place as S1 (Figure 6a) with a few secondary cracks. More detailed information can be obtained from Figures 6b and 6c. The intergranular section is also a main part in the crack initiation area, as shown in Figure 6b, which reveals the brittleness of the main fracture. The grain boundary is clean in the intergranular zone, and no features of hydrogen embrittlement and harmful precipitates were found. In the magnified picture (Figure 6c), fatigue features clearly appear, which imply a fatigue fracture. The fatigue expansion zone is a semicircle area with a radius of approximately 10 mm.

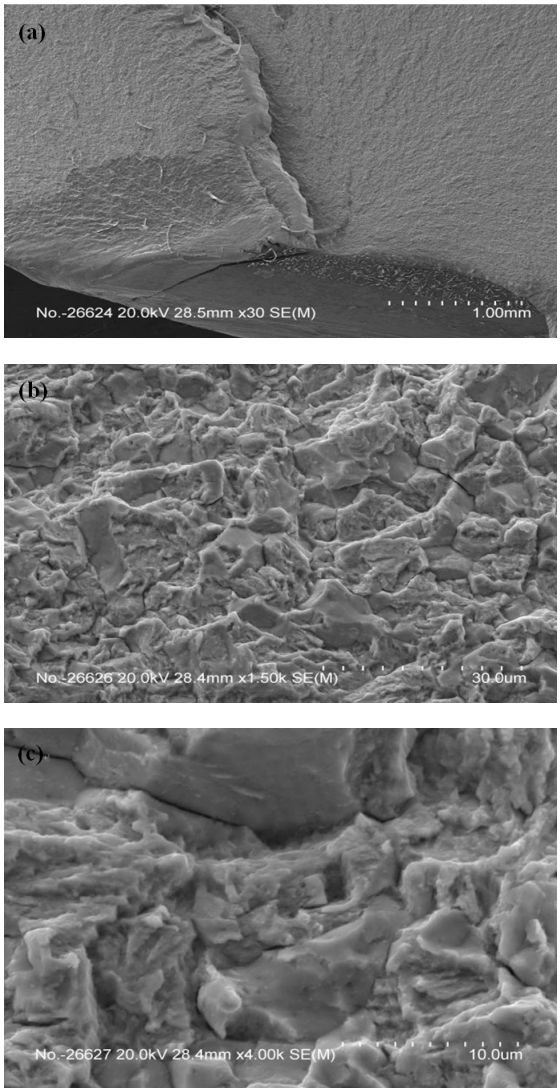

Figure 6. *SEM images of Fracture source region of S2: (a) Position of fracture source, (b) Low magnification of fracture source. (c) High magnification of fracture source.*

Figure 7 shows the region near the fatigue propagation zone, which cracked in a crisscross pattern with some parts cracked into pieces. This situation unquestionably shows that the part was working under complex and high three-dimensional stresses.

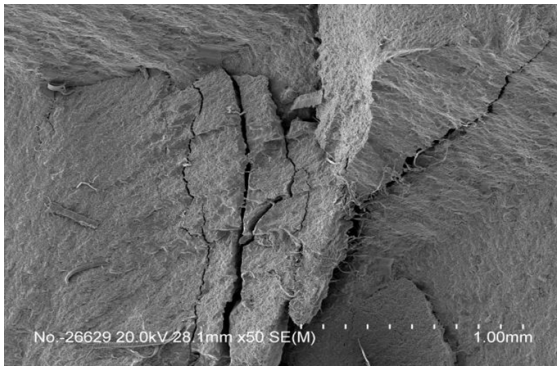

Figure 7. *The region with crisscross cracks near fatigue expansion zone of S2.*

The possibility of surface processing damage [14] or improper geometric design [15] can be ruled out after further confirmation on all samples including the fracture source and their side surface, since the fillet transition of the spline root and surface quality (roughness) nearby were proven to be normal. The phosphating film that covered the side surface of the spline root were also identified as normal, since no destructive abrasion damages were detected on it even after working time.

3.3. Metallographic Investigation

Samples S1 and S2 were made into metallographic specimens and treated by 4% NITAL to investigate the structure. The microstructures of all samples are tempered troostite, which is considered the required structure of spring steels [16]. The metallographic structures of S1 and S2 are shown in Figure 8. No structure defects such as inclusions and decarburization were detected.

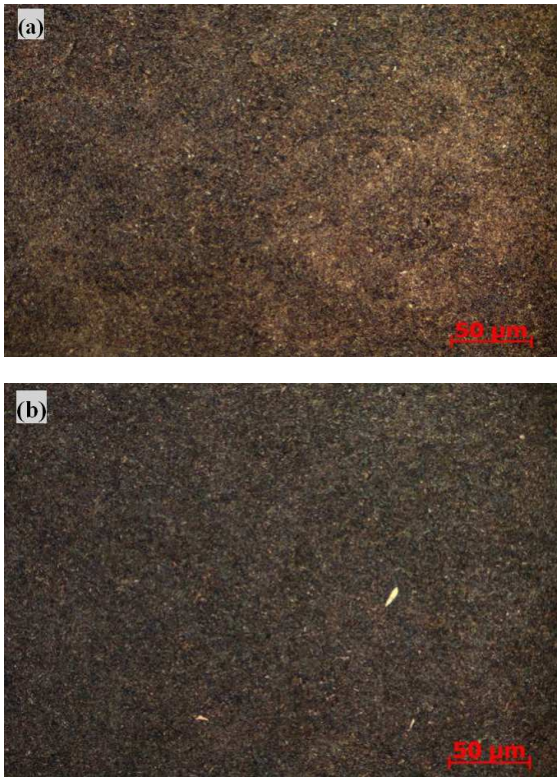

Figure 8. *Metallographic structures of S1 and S2: (a) Structure of S1, (b) Structure of S2.*

3.4. Hardness Test

The micro hardness values of S1 and S2 were obtained by Vickers scale with a load of 1 kg. Measuring positions were taken every 1 mm from the surface to the internal region (10 mm to the surface) on the cross section of the spline, since the boundary of the fatigue expansion zone is approximately 10 mm to the surface. Five data points were taken to obtain the mean value at each distance. According to the producer's standard, the core hardness of the spline part should be confined in the range of HRC 47~51 for $HV_1$468~527. The

measuring result (Figure 9) shows that the hardness of S1 ranges from $HV_1$496.03 to $HV_1$524.26 within the measuring distance and that of S2 varies from $HV_1$480.90 to $HV_1$518.57. The dramatic oscillation of hardness value is another evidence of inhomogeneous microstructures which might cause residual stress [17]. Furthermore, the hardness values of the near-surface region are very close to the upper limit, which proves again the insufficient tempering after the quenching process (refer to Figure 1). Apparently, the hardness result confirms the previous conclusion in *3.2*. If there is high residual stress caused by insufficient tempering, which causes unexpected brittleness, once the fatigue core is formed, the fatigue crack will rapidly propagate if there is a lack of deformation compatibility [18, 19].

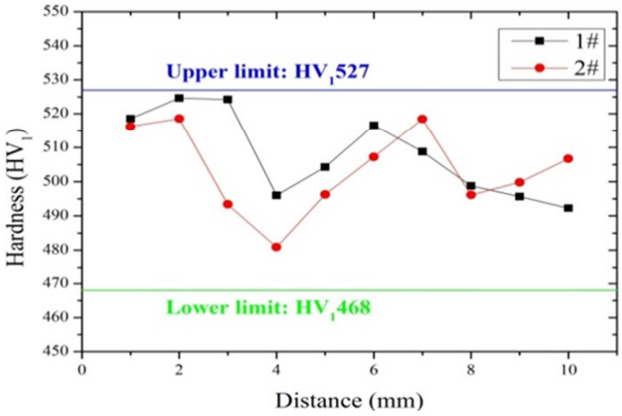

Figure 9. *Hardness values of fatigue expansion zone.*

3.5. Chemical Composition Investigation

The result of chemical composition of the torsion bar (S1) after the OES analysis is shown in Table 2, which is consistent with the GB3077-88 standard.

Table 2. *Chemical composition of torsion bar material.*

Elements	Sample	Specified (GB3077-88)
C	0.464	0.42-0.49
Si	0.318	0.17-0.87
Mn	0.707	0.50-0.80
P	0.0119	≤0.035
S	0.0017	≤0.035
Cr	0.969	0.80-1.10
Ni	1.627	1.30-1.80
Mo	0.236	0.20-0.30
V	0.1714	0.10-0.20

3.6. Tempering Simulation Experiment

All evidence has been pointed to insufficient tempering. If the brittle feature could be eliminated without dramatic oscillation of hardness distribution or significant change in metallographic structure type after tempering at medium temperature for a longer time, insufficient tempering time is undoubtedly the key factor to the failure [20]. Based on the heat preservation time (1.5 h) in the initial tempering cycle, a tempering simulation experiment with extended heat preservation time (3 h) was formulated by the producer as shown in Figure 10 without changing any other conditions: (1) Heat the sample to 380°C and maintain it at that temperature for 3 h; (2) rapidly cool the sample in the air to room temperature.

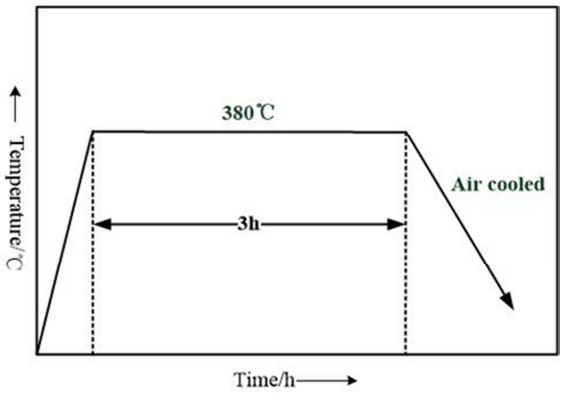

Figure 10. *Process of tempering simulation experiment.*

The tempering simulation experiment was performed on the spline coupons of S1 and S2; then, a hammer was used to make their artificial struck-fractures under normal stress, and an SEM analysis was performed to check the fracture property. A metallographic specimen of the retempered part was also prepared to check the metallographic structure. The results are shown in Figure 11. The brittle feature of the spline root area totally disappeared, since the artificial fractures of S1 and S2 are 100% large dimple ones as shown in Figures 11(a)-(b) instead of intergranular-dominant fractures. Furthermore, as shown in Figures 11(c)-(d), the microstructures of S1 and S2 after the tempering simulation experiment are still tempered troostite, which implies that our tempering simulation experiment did not induce a fundamental change in type of metallographic structure.

The next procedure was to investigate the hardness of the tempered sample. A spline root area within 10 mm to the surface on each sample was selected to measure the hardness values of S1 and S2. The results are illustrated in Figure 12. The brittleness-ductility transition appears to have been achieved at a small sacrifice of hardness. However, the hardness values were controlled in more reasonable range, and the hardness curves tend to become more uniform, which implies that proper and sufficient tempering time could eliminate the harmful brittleness and structure inhomogeneity of the spline root area.

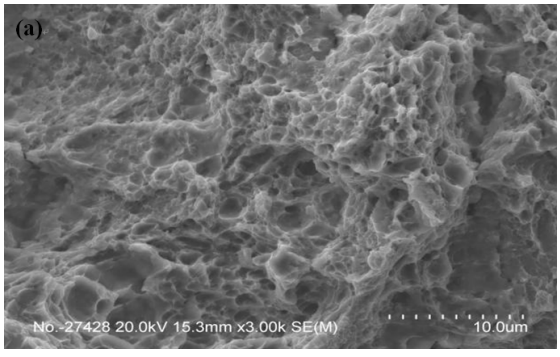

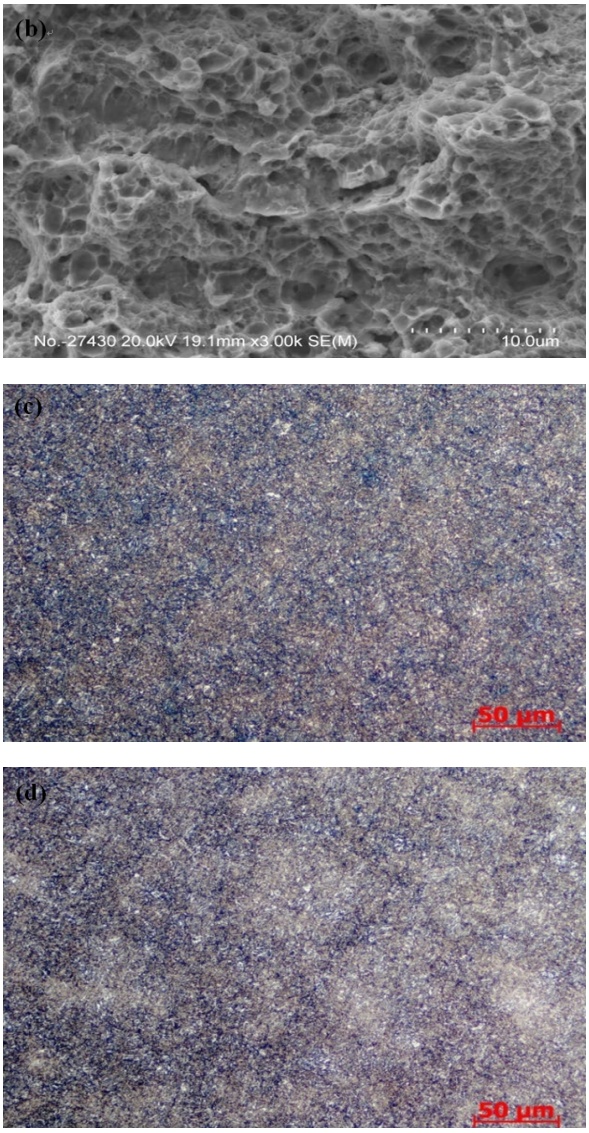

Figure 11. *SEM images of artificial-struck fractures and metallographic structure of spline part of S1 and S2 after tempering simulation experiment: (a) SEM image of struck fracture of S1, (b) SEM image of struck fracture of S2, (c) Metallographic structure of S1, (d) Metallographic structure of S2.*

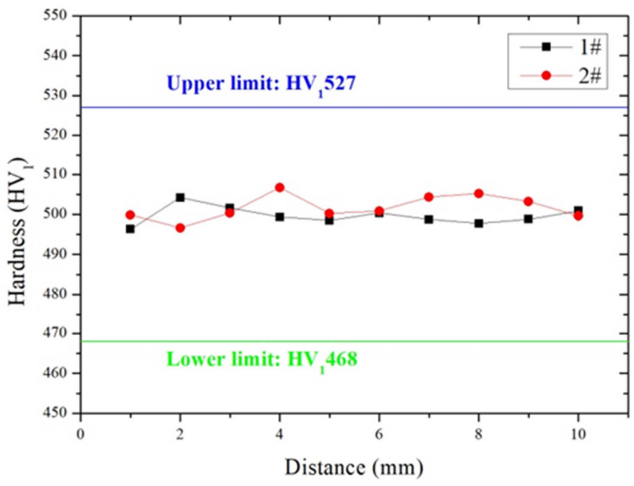

Figure 12. *Hardness values of spline root area on S1 and S2 after tempering simulation experiment.*

4. Comprehensive Discussion

Macroscopic observation on the fracture morphology reveals that the failed torsion bar (S1) was fractured by the same mechanism as referencing control sample (S2) in the fatigue test. The fracture initiation site is on the fillet of the spline root, where it is more easily to cause stress concentration. In addition, the ratchet pattern and 45° crack propagation from the shaft axis were found, which was generally identified as torsional-fatigue cracking. Further inspections such as SEM analysis, metallographic investigation and hardness test on the samples illustrate that the fractures truly initiated from the same place as shown in the macroscopic observation. Moreover, the fatigue propagation zones were proven to be brittle: there was a considerable proportion of intergranular areas in the fatigue propagation zone in a half circle area with the radius of approximately 10 mm, which is a very small area compared to the entire fracture. Hence, the part was working under extremely large stress, and the fatigue expansion process switched to an unstable propagation over a very short period of time. In other words, the period for fatigue nucleation was the major percentage of the entire fatigue life instead of the fatigue propagation time. The metallographic structure was proven to be tempered troostite as expected, and results of the hardness test in the fatigue expansion zone were nonuniform. Therefore, the untimely formation of the fatigue core and rapid propagation were direct consequences of the over-brittleness of the fatigue source and fatigue propagation zone since no surface processing defects or improper geometric designs on the spline part were identified. If the material is too brittle, the lack of strain compatibility will result in a high magnitude of local stress to promote crack initiation. Additionally, the grain boundaries and grain surfaces were quite clean; no features such as microholes, cross feet or obvious intergranular precipitates were detected on S1 and S2, which implies that the possibility of hydrogen embrittlement induced from hydrogen adsorption in the phosphating process or type-I temper embrittlement could be excluded.

In fact, insufficient tempering should be blamed for the fatal brittleness of the fatigue zone without doubt with supplementary results of tempering simulation experiment. After retempering coupons from S1 and S2, brittleness features were eliminated, and metallographic structures were ensured. Moreover, the hardness distribution near the surface of spline fillet was more uniform in the required range, i.e., extending tempering time can effectively eliminate over-brittleness and homogenize the microstructure.

5. Conclusion and Recommendation

The failure of the torsion bar during road tests was proven to be due to fatigue cracking under torsional stress. The fracture initiated from the side surface of the spline fillet, where a fatigue core prematurely formed and rapidly propagated due to the extremely large stress and over-

brittleness of the fatigue zone (approximately within 10 mm to the surface); therefore, the fatigue life was shortened. Insufficient tempering time was identified as the key factor of this fatal brittleness by performing a tempering simulation experiment under laboratory conditions based on the tempering process provided by the producer, since the intergranular fracture could be entirely replaced by a dimple fracture with no fundamental change in metallographic structure type. In addition, the hardness distribution became more uniform after retempering for a longer time. Hydrogen embrittlement and tempering embrittlement were not essential reasons for the failure.

The prevention of such problems depends on sufficient tempering to uniform the structure and eliminate large residual stress. From the view of this investigation, extending tempering time is recommended as an option to solve this problem.

Acknowledgements

The author expresses special thanks to financially support from the National Natural Science Foundation of China (21476179), the Foundation of Hubei Key Laboratory of Materials for New Energy Vehicles (Grant No. QCCLSZK2021A05, Hubei University of Automotive Technology) and the Foundation of Hubei Educational Committee (Grant No. B2019074).

References

[1] J. Yamakawa, K. Watanabe, A spatial motion analysis model of tracked vehicles with torsion bar type suspension. Journal of Terramechanics, 2004. 41 (2-3): pp. 113-126.

[2] G. P. S. Gagneza, S. Chandramohan, Estimation of Road Loads and Vibration Transmissibility of Torsion Bar Suspension System in a Tracked Vehicle. Journal of the Institution of Engineers (India), 2019, Ser. C. 100: pp. 747-761.

[3] S. A. Rodríguez, F. A. Quiceno, J. J. Coronado, Investigation of the failure of an automobile torsion bar. Journal of Failure Analysis and Prevention, 2009, 10 (1): pp. 11-17.

[4] V. Mocilnik, N. Gubeljak, J. Predan, Influence of presetting on fatigue lifetime of torsion bars. Procedia Engineering, 2011, 10: pp. 213-218.

[5] Zhiwei Yu, Xiaolei Xu, Zhi Yang, Yuanyuan Li, Case internal oxidation and intergranular fracture of carburized splined-shaft. Engineering Failure Analysis, 2012, 22: pp. 141-151.

[6] Xiaolei Xu, Zhiwei Yu, Failure analysis of a truck diesel engine crankshaft. Engineering Failure Analysis, 2018, 92: pp. 84-94.

[7] S. Zangeneh, M. Ketabchi, A. Kalaki, Fracture failure analysis of AISI 304L stainless steel shaft. Engineering Failure Analysis, 2014, 36: pp. 155-165.

[8] P. Peralta, C. Laird, Chap. 18-Fatigue of Metals, Physical Metallurgy, 5th ed., D. E. Laughlin, K. Hono, Ed., Elsevier, 2015, pp. 1765-1880.

[9] Taylor, D., CHAPTER 9 - Fatigue: Predicting Fatigue Limit and Fatigue Life, in the Theory of Critical Distances, 2007, Elsevier Science Ltd: Oxford. pp. 163-196.

[10] Taylor, D. CHAPTER 11 - Multiaxial Loading: Fracture and Fatigue Under Complex Stress States, The Theory of Critical Distances, 2007, Elsevier Science Ltd: Oxford. pp. 213-233.

[11] T. Sekercioglu, Failure analysis of torsion bar of projectile weaving machine. Journal of Failure Analysis and Prevention, 2010, 10 (5): pp. 363-366.

[12] Zhi Sun. Chap. 5-Failure Analysis of Fatigue Fracture, Failure Analysis: Fundamentals and Applications, 1st ed, 2005, China Machine Express: pp. 142-162 (in Chinese).

[13] Renzhi Wang, Peiyuan Wu. CMES, Chap. 4- Judgment of Fatigue Failure, Fatigue Failure Analysis, 1st ed, 1987, China Machine Express, pp 109-166 (in Chinese).

[14] Li Li, Youli Zhu, Yuanlin Huang, Fracture Failure Analysis of Torsion Bar with Surface Defects. China Surface Engineering, 2005, 01: pp. 47-49.

[15] I. Barsoum, F. Khan, Z. Barsoum, Analysis of the torsional strength of hardened splined shafts. Materials & Design, 2014, 54: pp. 130-136.

[16] Xueyuan Gong, Hongjun Dong, Fracture failure analysis of torsion bar spring. MW Metal Forming, 2022, 03: pp. 72-74.

[17] Xin Haohui, Correia José A. F. O., Veljkovic Milan et al. Residual stress effects on fatigue life prediction using hardness measurements for butt-welded joints made of high strength steels. International Journal of Fatigue, 2021, 147: 106175.

[18] D. McClaflin, A. Fatemi, Torsional deformation and fatigue of hardened steel including mean stress and stress gradient effects. International Journal of Fatigue, 2003, 26 (7): pp. 773-784.

[19] V. T. Troshchenko, Nonlocalized Fatigue Damage to Metals and Alloys. Materials Science, 2006, 42 (1): pp. 20-33.

[20] Xianwen Wang, Shuaijun Dong, Chaolei Zhang, Bo Jiang, Analysis of torsion bar failure occurring during the pre-strained manufacturing for heavy off-road tracked vehicles. Engineering Failure Analysis, 2022, 133: 105956.